INDIAN MONSOON

Indian monsoon derailed by a North Atlantic wavetrain

P. J. Borah[1,2], V. Venugopal[1,2,3]*, J. Sukhatme[1,2], P. Muddebihal[1], B. N. Goswami[4]

The forecast of Indian monsoon droughts has been predicated on the notion of a season-long rainfall deficit linked to a warm equatorial Pacific. Here we show that nearly half of all droughts over the past century differ from this paradigm in that they (i) occur when Pacific temperatures are near-neutral and (ii) are subseasonal phenomena, characterized by an abrupt decline in late-season rainfall. This severe subseasonal rainfall deficit can be associated with a Rossby wave from mid-latitudes. Specifically, we find that the interaction of upper-level winds with an episodic North Atlantic vorticity anomaly results in a wavetrain that curves toward East Asia, disrupting the monsoon. This atmospheric teleconnection offers an avenue for improved predictability of droughts, especially in the absence of telltale signatures in the Pacific.

Embedded in the interannual and intraseasonal variability of Indian summer monsoon rainfall (ISMR) (*1*–*4*) are complex space-time patterns pertaining to its extreme states, namely floods and droughts (*3*, *5*, *6*). Given that the socioeconomic fabric of one-sixth of the world's population is intricately tied to the state of the monsoon (*7*), these extremes, especially droughts, have a devastating impact on agriculture and the economy. Against this backdrop, despite its high potential predictability, the forecast of ISMR one season in advance remains a big challenge (*8*–*10*). For instance, it is known that anomalously warm waters in the equatorial central and eastern Pacific (El Niño) are associated with some ISMR droughts (*11*–*15*). However, what drives droughts not associated with an El Niño has remained mostly unknown. Further, the prevailing notion is that ISMR droughts are characterized by large-scale season-long rainfall deficit. Indeed, a deeper insight into droughts by way of their subseasonal evolution is essential not only for a better understanding of these extremes but also, practically, for targeted improvement of general circulation models in realizing the potential for improved ISMR prediction.

Over the past century, India has experienced 23 droughts and, as identified in table S1, 13 of these occurred with, and 10 without, an El

[1]Centre for Atmospheric and Oceanic Sciences, Indian Institute of Science, Bangalore 560012, India. [2]Divecha Centre for Climate Change, Indian Institute of Science, Bangalore 560012, India. [3]Interdisciplinary Centre for Water Research, Indian Institute of Science, Bangalore 560012, India. [4]Department of Physics, Cotton University, Guwahati 781001, India.
*Corresponding author. Email: venu.vuruputur@gmail.com or venu@iisc.ac.in

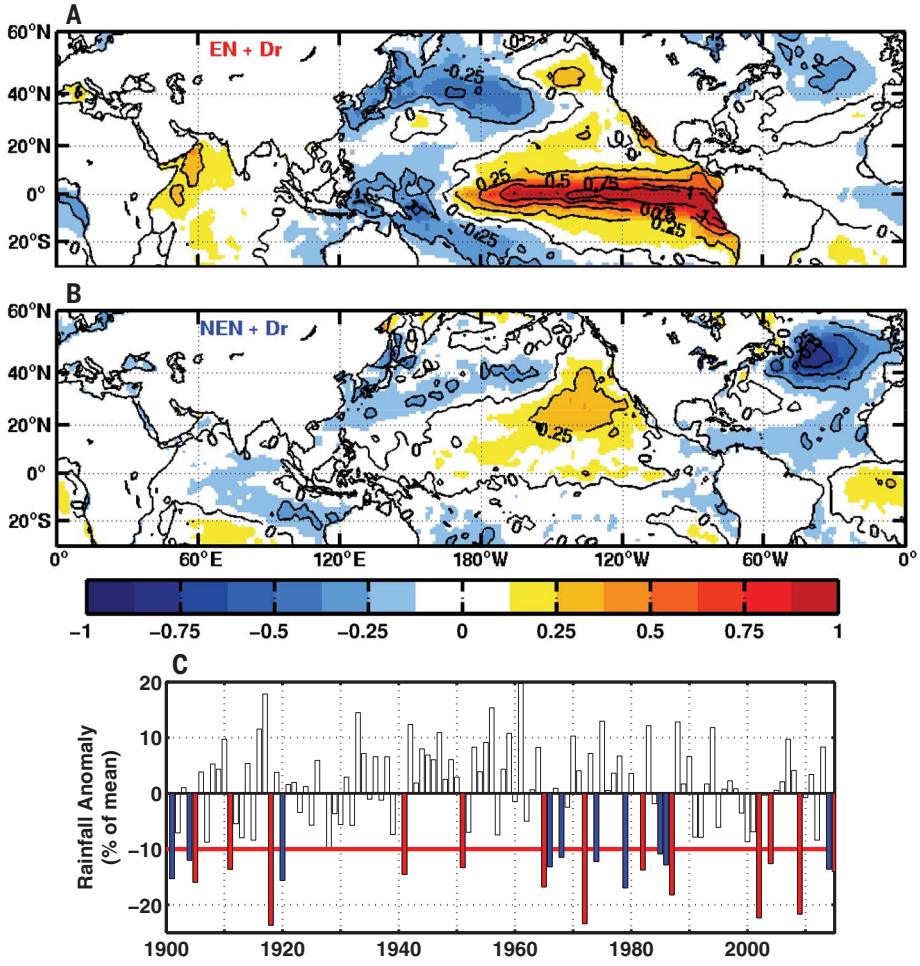

Fig. 1. Sea surface temperature and seasonal rainfall anomalies for the two types of Indian monsoon droughts. Spatial distribution of anomalies of detrended JJAS SST for the two types of Indian monsoon droughts. (**A**) EN + Dr and (**B**) NEN + Dr. The detrending is based on removal of a linear trend for the period 1901–2015 at each grid location, and the maps shown are the average of fluctuations around the trend, for the years listed in table S1. Based on one-degree monthly SST product from the Hadley Centre. Color bar is in degrees Celsius. (**C**) Interannual variation of anomalies of seasonal (JJAS) monsoon rainfall based on the Indian Institute of Tropical Meteorology homogeneous Indian monthly rainfall dataset for the period 1901–2015. The horizontal red line at −10% denotes the threshold for defining a drought, as per the India Meteorological Department (IMD). The departures marked in red (blue) indicate droughts that occurred during an El Niño (no El Niño) year. See methods in the SM.

Niño. These two types of droughts are henceforth referred to as EN + Dr and NEN + Dr (*16*), respectively. This sea surface temperature (SST)–based classification is confirmed in Fig. 1, A and B, which shows the mean of detrended SST anomalies during June through September (JJAS) for the years listed in table S1. Both types of droughts (Fig. 1C), although significantly different from normal years, are statistically indistinguishable from each other at a 5% significance level ($P = 0.09$) on a seasonal scale (fig. S1). This similar final seasonal state in the two categories of droughts, in the face of disparate oceanic conditions (warm versus neutral Pacific), prompts us to investigate their subseasonal evolution.

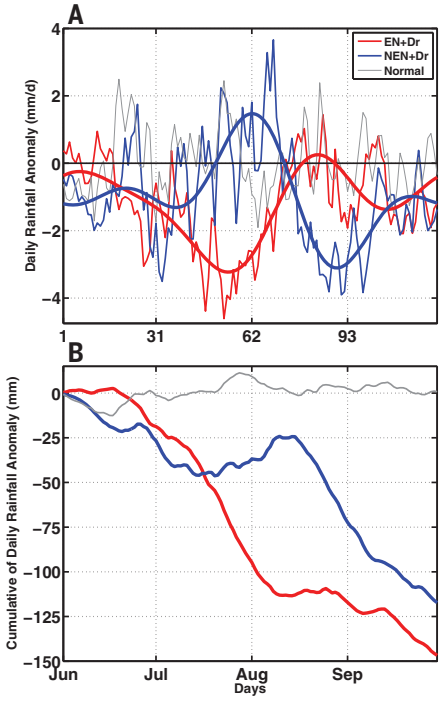

Fig. 2. Daily rainfall anomalies and their cumulative for the two types of droughts. (**A**) Temporal evolution of anomalies of daily area-averaged rainfall over central India (16.5°N to 26.5°N, 74.5°E to 86.5°E; land only) during JJAS, for the two categories of droughts, along with their respective leading harmonics (~120, 60, and 40 days; thick red and blue curves). The thin red and blue curves shown are an average of daily anomalies of 13 EN + Dr and 10 NEN + Dr years listed in table S1. (**B**) Cumulative daily rainfall shown in (A). The average daily rainfall anomalies for a normal year (based on 18 randomly chosen years with a seasonal rainfall anomaly between −5 and 5%) and its cumulative are shown as a gray line in both panels. Based on IMD gridded one-degree daily rainfall data from 1901 to 2015. See methods in the SM.

Figure 2A shows the temporal behavior of daily anomalies of area-averaged central India rainfall [16.5°N to 26.5°N, 74.5°E to 86.5°E; see the methods section in the supplementary materials (SM)] during JJAS, for the two drought types, in comparison to normal years. The daily anomalies for each of the drought years are shown in fig. S2, from which the averages shown in Fig. 2A are estimated. The difference in the evolution of the two drought types is immediately evident. Specifically, in the EN + Dr category (Fig. 2A, thin red curve), negative rainfall anomalies, that is, departures from the daily climatological mean, set in during mid-June and persist till early August. On the other hand, in NEN + Dr (Fig. 2A, thin blue curve), anomalies have more rapid and intense fluctuations culminating in a sharp drop (see long break highlighted by the blue ellipse in fig. S2B) during mid-August. It is this break in late August that drives the monsoon into a state of drought. The envelopes (Fig. 2A, thick curves) of these two types of droughts, represented by their respective leading harmonics (~120, 60, and 40 days), reinforces this distinction.

The difference in timing and duration of the breaks in these two categories is amplified in Fig. 2B, which shows the respective composites of the cumulative daily rainfall anomalies (see fig. S3 for individual years). A comparison of these composites also shows that NEN + Dr has a larger overall deficit than EN + Dr until early July. In sharp contrast, during the core of the monsoon season (July to mid-August), while the deficit persists and deepens in EN droughts, rainfall is near to above normal in NEN + Dr. This apparent recovery in the latter category is interrupted by the sudden break in mid-August. Although the timing of the deficits may be different, the rate of change (drop) in both categories is ~2 to 2.5 mm per day (0 to −100 mm in ~45 days during June and July for EN + Dr versus −25 to −75 mm in 20 days during mid to late August for NEN + Dr). The final state of the two curves in Fig. 2B is in agreement with the fact that, on average, the magnitude of the seasonal deficit is larger in EN + Dr (17%) than in NEN + Dr (13%), as can be inferred from table S1. While the discussion so far has revolved around the rainfall in central India, the contrast holds for all of India as well (fig. S4).

The temporal evolution of rainfall in the two categories of droughts has an associated spatial footprint. Figure 3 shows the spatial patterns of the composites of cumulative daily rainfall anomalies on a 20-day time scale for the two categories of droughts. What stands out here is that in EN + Dr, negative rainfall anomalies appear near the foothills of the Himalayas and Gangetic plains (also, Western Ghats) and then propagate southward. Once the deficit sets in, it persists and covers most of the country by the end of July. Despite the minor recovery during August in the north central plains—corresponding to positive rainfall anomalies in Fig. 2A or, equivalently, the flattening of the cumulative (red) curve in Fig. 2B—the deficit during June and July is sufficient for the season to end in a drought. In contrast, for NEN + Dr, below-normal rainfall in June is largely confined to the west central plains. This is followed by a period when most of the country experiences above-normal rainfall (Fig. 3, I and J, mid-July to mid-August). This path to a near-normal state is derailed by a deficit that appears in the central plains and rapidly expands to cover the entire country within 20 days (Fig. 3K, 20 August to 8 September). Our analysis thus clearly shows that while EN droughts are a consequence of a deficit that persists through the season, NEN droughts are subseasonal phenomena with a moderate early-season deficit compounded by an abrupt decline in late-season rainfall.

The apparent stranglehold of the equatorial Pacific on Indian monsoon variability (in particular, droughts) has been extensively documented (*13*, *14*, *17*). Here we focus on the droughts belonging to the latter category (NEN + Dr), which occur in the absence of anomalously warm waters in the Pacific (Fig. 1B). Specifically, we investigate the late-August break that derails the monsoon, by considering the period when the gradient of rainfall decline is steepest (Fig. 2, blue curves). The anticyclonic lower-level circulation over India confirms the break period (Fig. 4, C and D). Looking outward from India, a standout feature in the atmosphere is the presence of a strong, upper-level cyclonic circulation to the west, in the North Atlantic region (Fig. 4A). Note that this summertime feature is deep tropospheric (fig. S5) (*18*, *19*) and has a tendency to occur episodically in June and August with a duration of 2 to 3 weeks (fig. S6B, blue curve; see also the supplementary text section in the SM).

The interaction of upper-level winds and this vorticity anomaly, as seen in the 200 mbar meridional wind anomalies (shading in Fig. 4A), indicates a wavetrain to the east of the Atlantic that extends all the way to East Asia (*20*, *21*). At 500 mbar (Fig. 4B), the wavetrain curves toward the equator, with a prominent signature over the Indian region, apparently guided by the Tibetan plateau (the narrowing of the wind anomalies to the east of 60°E in Fig. 4B). Finally, the anticyclonic nature of wind anomalies over northern India, signs of which are evident at 500 mbar, becomes clearer at lower levels (700 and 850 mbar; Fig. 4, C and D). This circulation anomaly not only weakens the zonal flow over the Arabian Sea (i.e., disrupting the Somali jet) but also strengthens and spreads to cover all

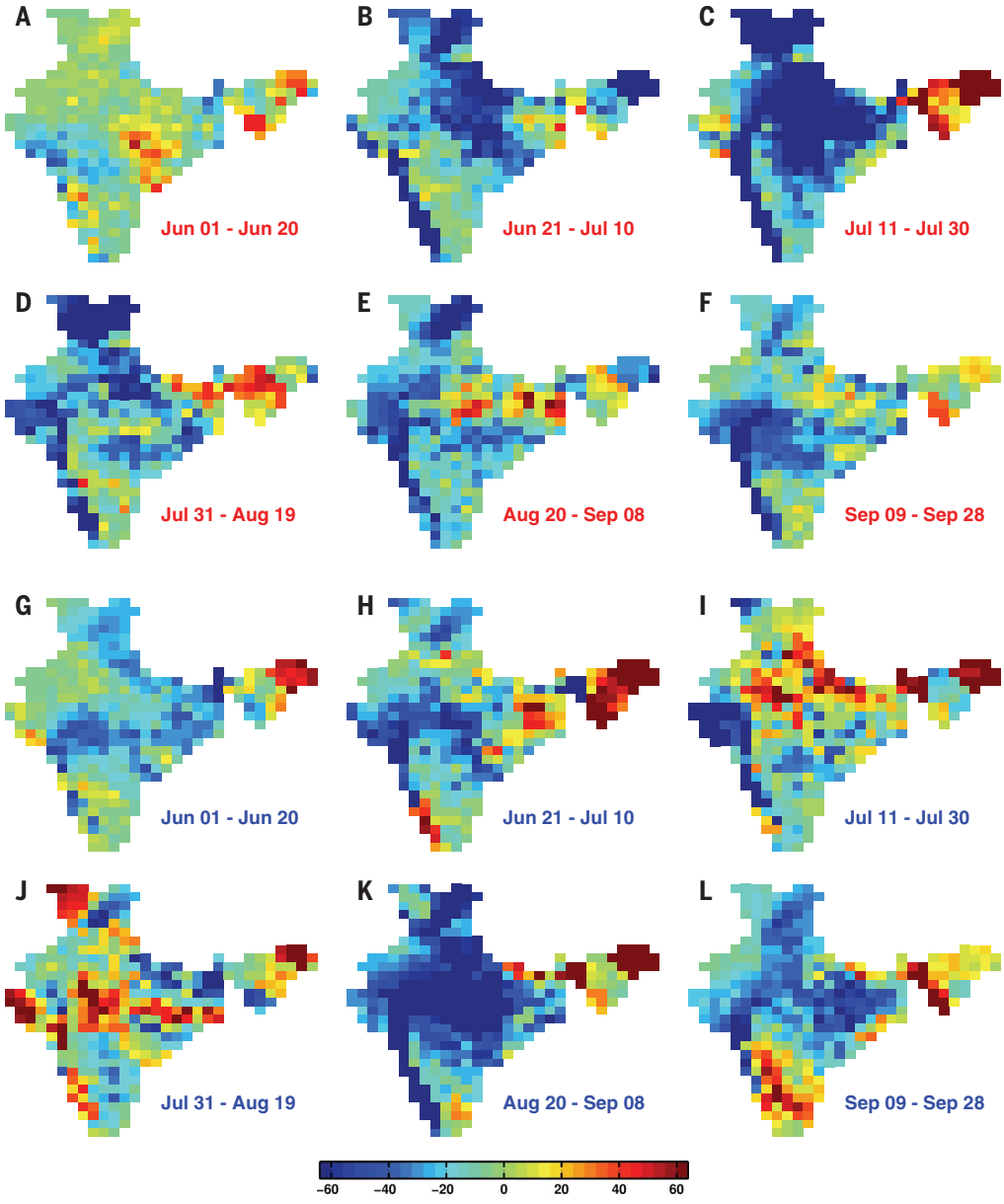

Fig. 3. Spatial distribution of cumulative rainfall anomalies on a 20-day time scale. (**A** to **F**) EN + Dr (top two rows) and (**G** to **L**) NEN + Dr (bottom two rows). The anomalies shown are composites based on 13 EN + Dr and 10 NEN + Dr years, respectively (see table S1). Color bar is in millimeters.

of India, as one descends from 700 to 850 mbar. Contrasting this with the low-level cyclonic circulation over India 20 days prior to the break (fig. S7) highlights the abruptness of this phenomenon (Fig. 3, J and K). Thus, the late-season decline in rainfall can be associated with a large-scale Rossby wave from the North Atlantic to the Indian subcontinent.

The wide-ranging influence of mid-latitudes on the tropics includes the initiation and variability of the Indian monsoon (*22*–*24*), monsoon bursts in Australia (*25*), and short-duration extremes in both hemispheres (*26*). The atmospheric teleconnection and its impact identified in our work are consistent with the recent recognition of the role played by mid-latitude Rossby waves in affecting tropical climate at seasonal and shorter-duration time scales (*26*–*28*). In addition, our diagnostic analysis brings forth two intriguing aspects that call for further scrutiny: First, most NEN droughts seem to coincide with years when the North Atlantic was anomalously cold (fig. S6A); and, second, there appears to be a significantly higher likelihood of episodes of cyclonic vorticity anomalies over cold summer waters (see supplementary text, fig. S6B, and table S2). Both of these associations are statistical in nature and do not imply causality, especially as it is difficult to excite a large-scale atmospheric response to SST anomalies in the mid-latitudes (*29*, *30*). Together, they raise the possibility that there might be an overarching common element behind the excitation and sustenance of cold SSTs and uncharacteristically long duration vorticity anomalies during the summer in the North Atlantic region.

The association of the Atlantic basin with the Indian monsoon in particular has been explored in great detail, albeit mostly on decadal and interannual time scales (*31*–*36*). However, the subseasonal atmospheric bridge identified in this study represents a potentially new pathway in our understanding of monsoon droughts, especially when the

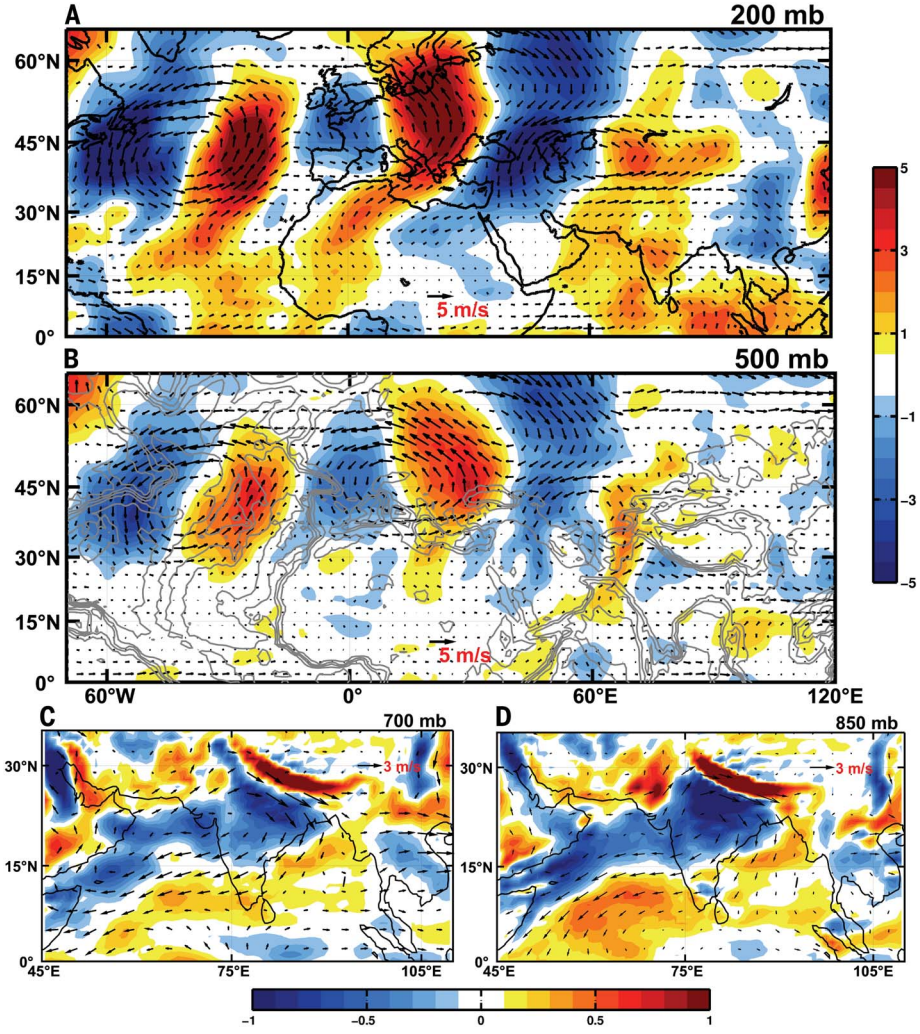

Fig. 4. Wind and vorticity anomalies during the late-August break in NEN droughts. Composites of anomalies of (top two panels) wind (vectors) and meridional velocity (shading) at (**A**) 200 mbar and (**B**) 500 mbar during the first half of the break (days 81 to 90; blue curve in Fig. 2B) in the Indian monsoon rainfall; and (bottom two panels) wind (vectors) and vorticity ($\times 10^5$; shading) at (C) 700 mbar and (D) 850 mbar, based on the respective break periods late in the season for each of the NEN + Dr years. The gray lines in the 500 mbar panel represent topography. Based on ERA 20th Century Reanalysis data. See methods in the SM.

equatorial Pacific temperatures are near-neutral. More pertinently, it points to the need for expanding the existing tropics-centered paradigm of monsoon droughts into a framework that includes extratropical teleconnections (*37*).

REFERENCES AND NOTES

1. B. Parthasarathy, D. A. Mooley, *Mon. Weather Rev.* **106**, 771–781 (1978).
2. V. Krishnamurthy, J. Shukla, *J. Clim.* **13**, 4366–4377 (2000).
3. S. Gadgil, *Annu. Rev. Earth Planet. Sci.* **31**, 429–467 (2003).
4. C. D. Hoyos, P. J. Webster, *J. Clim.* **20**, 4402–4424 (2007).
5. D. Sikka, "Monsoon drought in India," *Tech. Rep. 2*, COLA/CARE, Maryland, USA (1999).
6. B. N. Goswami, in *Intraseasonal Variability in the Atmosphere-Ocean Climate System*, W. K.-M. Lau, D. E. Waliser, Eds. (Springer Praxis Books, Springer, ed. 2, 2012), pp. 21–72.
7. S. Gadgil, S. Gadgil, *Econ. Polit. Wkly.* **41**, 4887–4895 (2006).
8. R. S. Nanjundiah, P. A. Francis, M. Ved, S. Gadgil, *Curr. Sci.* **104**, 1380–1393 (2013).
9. B. Wang *et al.*, *Nat. Commun.* **6**, 7154 (2015).
10. J. Li, B. Wang, *Clim. Dyn.* **46**, 2847–2861 (2016).
11. E. M. Rasmusson, T. H. Carpenter, *Mon. Weather Rev.* **111**, 517–528 (1983).
12. P. J. Webster *et al.*, *J. Geophys. Res. Oceans* **103**, 14451–14510 (1998).
13. K. K. Kumar, B. Rajagopalan, M. Hoerling, G. Bates, M. A. Cane, *Science* **314**, 115–119 (2006).
14. A. G. Turner, H. Annamalai, *Nat. Clim. Chang.* **2**, 587–595 (2012).
15. F. Fan *et al.*, *Atmos. Sci. Lett.* **18**, 175–182 (2017).
16. H. Varikoden, J. V. Revadekar, Y. Choudhary, B. Preethi, *Int. J. Climatol.* **35**, 1916–1925 (2014).
17. X. Li, M. Ting, *Geophys. Res. Lett.* **42**, 3502–3512 (2015).
18. T. Palmer, S. Zhaobo, *Q. J. R. Meteorol. Soc.* **111**, 947–975 (1985).
19. C. Wang, *Clim. Dyn.* **53**, 5119–5136 (2019).
20. B. J. Hoskins, G.-Y. Yang, *J. Atmos. Sci.* **57**, 1197–1213 (2000).
21. G. Branstator, J. Teng, *J. Atmos. Sci.* **74**, 1513–1532 (2017).
22. S. Bordoni, T. Schneider, *Nat. Geosci.* **1**, 515–519 (2008).
23. R. Krishnan, V. Kumar, M. Sugi, J. Yoshimura, *J. Atmos. Sci.* **66**, 553–578 (2009).
24. R. K. Yadav, *Clim. Dyn.* **32**, 549–563 (2009).
25. S. Narsey, M. J. Reeder, D. Ackerley, C. Jakob, *J. Clim.* **30**, 5377–5393 (2017).
26. N. Boers *et al.*, *Nature* **566**, 373–377 (2019).
27. Y.-K. Lim, *Clim. Dyn.* **44**, 3211–3222 (2015).
28. L. O'Brien, M. J. Reeder, *Q. J. R. Meteorol. Soc.* **143**, 2374–2388 (2017).
29. Y. Kushnir, I. M. Held, *J. Clim.* **9**, 1208–1220 (1996).
30. Y. Kushnir *et al.*, *J. Clim.* **15**, 2233–2256 (2002).
31. B. N. Goswami, M. S. Madhusoodanan, C. P. Neema, D. Sengupta, *Geophys. Res. Lett.* **33**, L02706 (2006).
32. R. Lu, B. Dong, H. Ding, *Geophys. Res. Lett.* **33**, L24701 (2006).
33. M. Rajeevan, L. Sridhar, *Geophys. Res. Lett.* **35**, L21704 (2008).
34. C. Wang, F. Kucharski, R. Barimalala, A. Bracco, *Meteorol. Z. (Berl.)* **18**, 445–454 (2009).
35. L. Krishnamurthy, V. Krishnamurthy, *Clim. Dyn.* **46**, 2269–2285 (2016).
36. C. T. Sabeerali, R. S. Ajayamohan, H. K. Bangalath, N. Chen, *Geophys. Res. Lett.* **46**, 4460–4467 (2019).
37. C. Stan *et al.*, *Rev. Geophys.* **55**, 902–937 (2017).

ACKNOWLEDGMENTS

We thank R. S. Nanjundiah, J. Srinivasan, D. Sengupta, and D. S. Battisti for useful discussions; J. M. Wallace, R. Roca, and A. H. Sobel for constructive suggestions on improving the narrative; and R. Matthew for providing seasonal anomalies of monsoon rainfall over the homogeneous regions. We thank IMD, UK Met Office, and ECMWF for daily gridded rainfall, monthly gridded SST, and ERA 20th Century Reanalysis datasets, respectively. **Funding:** P.J.B. thanks the Department of Science and Technology (DST), Government of India (GoI), for support under the INSPIRE PhD fellowship (IF160707). V.V. and J.S. thank DST, GoI, for financial support (DST/CCP/NCM/75/2017) under their Climate Change Programme. V.V. thanks the Ministry of Earth Sciences, GoI, for their support under the project (MOES/PAMC/H&C/41/2013-PC-II) "Advanced Hydrologic Research and Knowledge Dissemination." J.S. thanks the University Grants Commission, GoI, for support under the Indo-Israel Joint Research Programme (F 6-3/2018). B.N.G. thanks the Science and Engineering Research Board, GoI, for the SERB Distinguished Fellowship. **Author contributions:** V.V. formulated the initial question of dominant drought patterns. P.M. performed the preliminary set of computations with monthly rainfall. P.J.B. performed all subsequent calculations with daily data. V.V. and J.S. were involved in all of the analysis and interpretation and took the lead in writing the manuscript. B.N.G contributed to the interpretation and writing of the manuscript. **Competing interests:** The authors declare no competing interests. **Data and materials availability:** Data sources and their access has been provided in the data and methods section in the SM.

SUPPLEMENTARY MATERIALS

science.sciencemag.org/content/370/6522/1335/suppl/DC1
Data and Methods
Supplementary Text
Figs. S1 to S7
Tables S1 and S2
References (*38*–*43*)

4 July 2019; accepted 21 October 2020
10.1126/science.aay6043

Indian monsoon derailed by a North Atlantic wavetrain

P. J. Borah, V. Venugopal, J. Sukhatme, P. Muddebihal and B. N. Goswami

Science **370** (6522), 1335-1338.
DOI: 10.1126/science.aay6043

Season of the drought

The Indian monsoon is a critical source of water for hundreds of millions of people, and when it fails to deliver its normal quantity of rain, enormous human, economic, and ecological costs can be incurred. Monsoon droughts are not always seasonal, however. Borah *et al.* found that nearly half of all monsoonal droughts were subseasonal and characterized by a steep decline in late-season rainfall. Moreover, this type of subseasonal drought appears to be related to a distinct cold anomaly in the North Atlantic Ocean, raising the possibility that monsoon droughts may be more predictable.

Science, this issue p. 1335